A Modular SiC High-frequency Solid-state Transformer for Medium Voltage Applications

Dong Dong, *Member, IEEE*; Mohammed Agamy, *Senior Member, IEEE*; Ravisekhar Raju*, Member, IEEE;* Jovan Bebic*, Member, IEEE;* Qin Chen, *Member, IEEE*; Gary Mandrusiak

***Abstract*— The advancements in wide-band-gap (WBG) devices are enabling applications of power electronic converters coupled directly to medium voltage and incorporating galvanic insulation within the converter using high-frequency solid-state transformers. This paper presents analysis, design and the characterization results of a 50 kVA modular soft-switched ac-ac solid-state transformer using SiC MOSFET for MV (>6 kV ac) applications. The solid-state transformer is comprised of two hard-switched ac-line interfaces and a resonant dc-dc stage switched around 180 kHz. To minimize the cost of switching elements per ampere and maximize design flexibility, the design uses multiple discrete SiC devices of, readily available, 1700 V ratings. The paper covers the analysis of soft-switching operation, control architecture, converter design, and system level integration.**

***Index Terms*— Solid-state transformer, soft-switching, SiC.**

I. INTRODUCTION

Compared to the conventional line-frequency transformer, solid-state transformer (SST), or power electronic transformer (PET) is a technology of transferring electrical power through a small high-frequency transformer of which the flux linkage is established by the switching power converters rather than the grid voltage [1-5]. The high-frequency operation of power converters reduces the maximum flux, leading to a smaller magnetic core size and weight. Assuming appropriate insulation, SST can be used as a stackable modular power electronic building-block (PEBB) to build different types of static power conversion equipment [6]. One attractive application for PEBB is direct medium voltage (MV) grid connection of power electronic converters serving low voltage (LV) load [7]. An example topology, showing series connected ac-dc PEBB connected in series on the AC side and in parallel on the DC side is shown in Fig. 1. Notwithstanding its size and weight advantages, the key challenge for industry to adopt SST in MV applications are cost and reliability of the high-frequency transformer, which ultimately drives the requirement of power electronics around it.

The material and labor-intensive assembly cost of high-frequency high power transformer contributes a large portion to the total cost. Nowadays in high power (>50 kVA) SST applications, the switching-frequency is usually less than 20 kHz and the typical transformer magnetic materials are Nanocrystalline or Amorphous due to its high flux permeability [3-5, 8-12]. However, the limited vendors and small volumes of such materials impede the cost reduction. To make SST economically viable, the low-cost ferrite magnetics with standard shapes are desired, which demands the switching frequency of power electronics above 100 kHz to fully exploit the ferrite materials [13]. In addition, pushing higher terminal voltage of single transformer by using high-voltage device (>1.2 kV) helps drive down the cost per kVA rating.

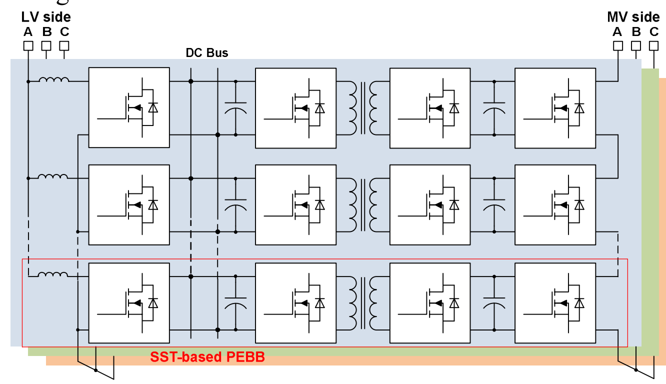

Fig. 1: MV grid-connection using SST based PEBB.

To use SST as PEBB in MV application, the insulation system of high-frequency transformer significantly impacts the power rating as well as reliability. High frequency transformer insulation must satisfy the requirements for electrical isolation, heat dissipation, and compact physical size. The mechanical, thermal, and magnetic coupling considerations generally demand thinner insulation. On the other hand, however, in grid application, the basic insulation level (BIL) requirement [14], i.e., impulse voltages representing waveforms during lightning strikes, poses a very significant design challenge. For example, for 4.16 kV and 13.8 kV system voltage levels, the transformer should meet at least 30 kV and 95 kV BIL level, respectively. Besides surviving short-duration voltage transients, the insulation must maintain the electrical isolation over the service life. Due to the voltage-induced acceleration of insulation failure, which is particularly significant under higher frequencies, the electric field in the insulation must be sufficiently low. Thicker insulation would lead to higher BIL and continuous operation voltage levels. Besides the thickness, the lateral dimension of the insulation must also be large enough to satisfy the requirements for the creepage, clearance, striking distances. Therefore, the less number of turns is desired to reduce the winding loss and winding size which leaves more room for insulation system. This will further require the converter to operate at very high frequency.

Based on both cost, thermal and insulation requirement of the transformer, high-voltage and high power, high frequency > 100 kHz but high efficiency power electronics solution is desired. This drives the adoption of high-voltage wide-band-gap (WBG) devices, e.g., 1.7 kV and 2.5 kV SiC MOSFETs, in modular SST PEBB applications. This paper focuses on the design and analysis of a very high frequency (around 200 kHz) ac-ac soft-switched solid-state transformer module, suitable for medium voltage (>6kV) applications. The power electronics was built by using paralleled 1.7 kV discrete SiC MOSFETs to achieve a highly scalable solution for SST applications with different power and voltage ratings.

II. Topology and Operation Analysis

As shown in Fig. 2, the modular solid-state transformer consists of three building blocks: two hard-switched H-bridges (outer-bridge) interfacing with the ac output and a bi-directional isolated dc-dc stage (inner-bridge) driving a high-frequency transformer. The switching frequency of the inner bridges and the ac-line bridges are listed in Table 1.

Table I Switching frequency in modular SST module

Inner bridge f_{sw_i}	Outer bridge f_{sw_l}
200~250 kHz	5~25 kHz

There are two major topology options for the bi-directional isolated dc-dc converter: resonant soft-switched topology [15-18] and dual-active bridge (DAB) [19-21]. As shown in Fig. 2, the bi-directional soft-switched CLLC type resonant topology is chosen in this paper to minimize the switching loss across the entire operation range and maximize the transformer power delivery capability with the smallest current harmonics. To achieve the identical design of power electronics hardware on both sides, the transformer ratio is chosen as 1:1, which also minimizes the common-mode (CM) *dv*/*dt* voltage stress across the primary and secondary-side windings, thereby reducing the CM noises.

The soft-switching dc-dc stage being running at fixed switching frequency close to its resonant frequency presents a unique characteristic similar as a dc-type transformer, well known as solid-state transformer (SST). The power regulation of such transformer is thereby controlled by the hard-switched H-bridges.

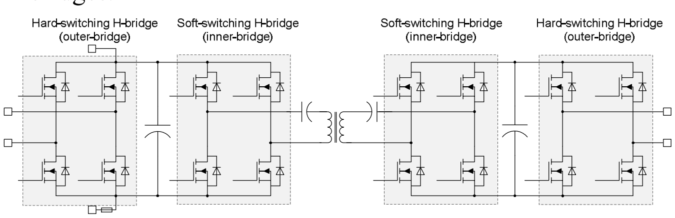

Fig. 2: AC-DC SST topology using H-bridge Converter.

A. Operational Analysis

There are two fixed-frequency control methods for the bi-directional soft-switching resonant converter, the key component of the modular SST. As shown in Fig. 3, the first method generates two sets of gating signals: 50% duty-cycle gating on the sending-side but synchronous rectification (SR) gating on the receiving-side [22]. Using this method, the receiving-side devices will receive OFF signals prior to the sending-side, which transfers the current to the body-diodes on the receiving-side. When the transformer current reaches zero, the receiving-side will stop conducting current and create a small reverse-recovery loss from the body-diodes. The magnetizing current then will be solely circulated on the sending-side to discharge the device junction capacitors during dead-time for zero-voltage-switching (ZVS). This is a typical control method for the LLC circuit. Fig. 4 illustrates the involved sending and receiving side devices in one switching period with a such control method. The critical time-points labeled in the figure are illustrated as follows.

T1: Receiving-side current returns to zero, diode rectifier stops conducting current; T2: Sending-side top device is turned off and the magnetizing current discharges the sending-side bottom device junction capacitor; T3: Sending-side bottom device voltage drops to zero during dead-time; T4: Sending-side bottom device is turned on under ZVS; T5: Remove receiving-side top device gate signal to let body diode conduct current.

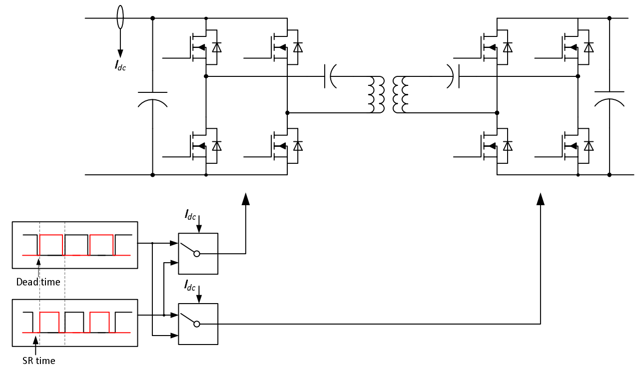

Fig. 3: Control methods of using 50% duty-cycle pulse SR signals.

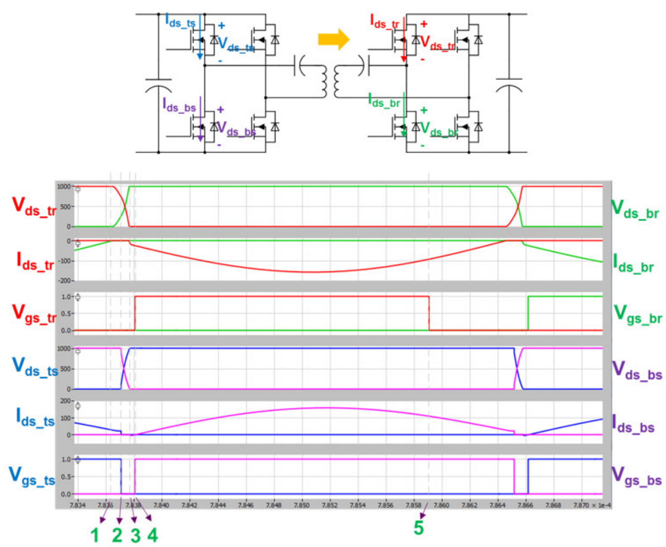

Fig. 4: Devices voltage and current in one switching period with 50% duty-cycle plus SR signals (with exaggeration on timing).

The first control method operates this bi-directional isolated dc-dc converter as a LLC circuit, thereby following the same design rule, e.g., magnetizing inductance, dead-time and the tuning procedure. However, it requires an extra current sensor to measure the power which swaps the gating signals between primary and secondary side when the power flow reverses the direction.

As shown in Fig. 5, the second control method applies the same 50% duty-cycle gating signals on both sides. All the devices will rely on the magnetizing current to discharge the device junction capacitors for ZVS. The method significantly simplifies the control and eliminates the additional current sensor. On the other side, however, it shows a different switching transition behavior and requires a different design procedure. Fig. 6 shows the one switching cycle simulation waveform of the involved phase-legs on two sides.

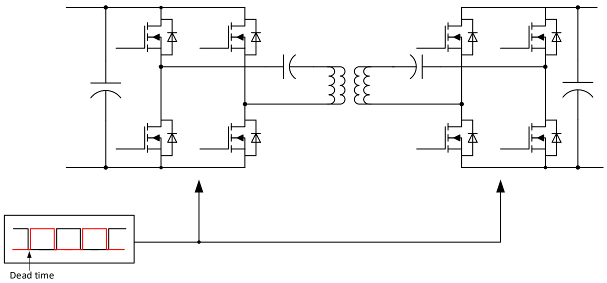

Fig. 5: Control method of using 50% duty-cycle signals on both side.

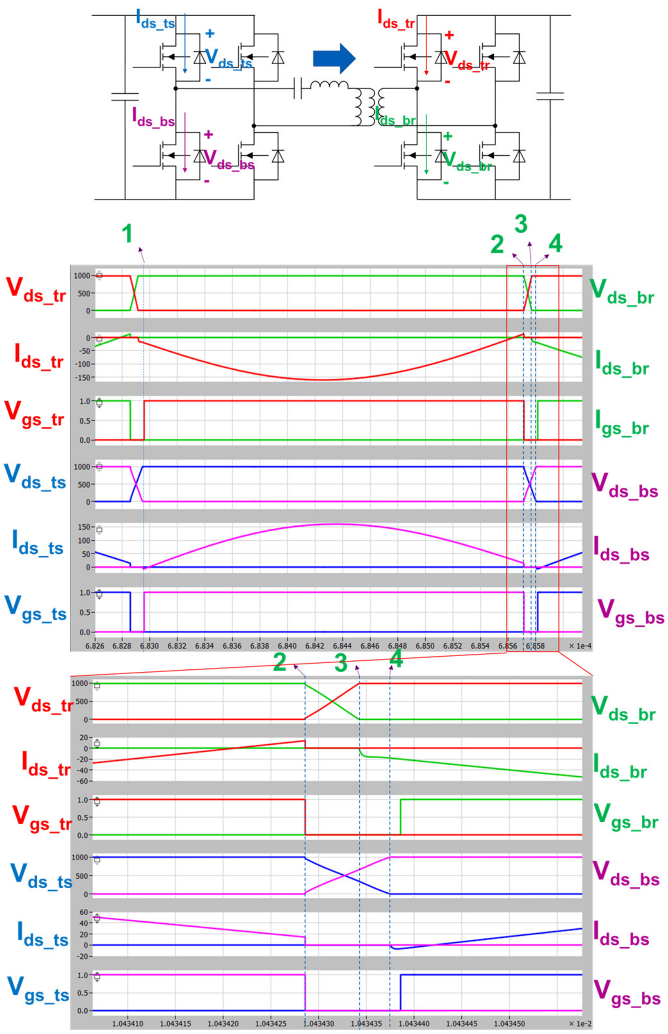

Fig. 6: Devices voltage and current in one switching period with 50% duty-cycle.

As shown in Fig. 6 and 7, from T1 to T2, the transformer current I_r flows from the sending-side to receiving-side. As the devices on both sides are controlled by the same signals, both sending and receiving-side dc-link capacitors will supply the magnetizing current I_{mag_s}, I_{mag_r}. Therefore, as shown in (1) and (2), the current through the sending-side and the receiving-side devices are slightly different due to the magnetizing current.

$$I_{ds\_ts} = I_{tr} + I_{mag\_s} \tag{1}$$

$$I_{ds\_tr} = I_{tr} - I_{mag\_r} \tag{2}$$

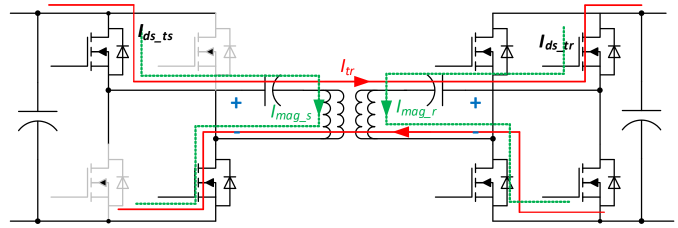

Fig. 7: Current path for bi-directional resonant converter during power transfer.

Due to the symmetry on two sides of the high-frequency transformer, the magnetizing currents supplied by two sides will be close to each other.

$$I_{mag\_s} = I_{mag\_r} = 0.5 I_{mag} \tag{3}$$

Assumes the switching frequency is equal or slightly lower than the resonant-frequency. When the resonant current reaches zero, as all involved devices are still gated, the current I_{tr} will continue to flow in the opposite direction, as show in Fig. 8.

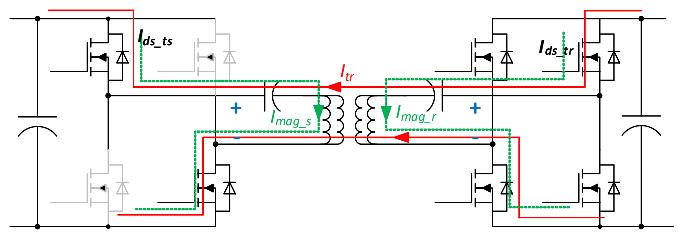

Fig. 8: Current path for bi-directional resonant converter when the resonant current reverses direction.

When both top devices are turned off at T2, the current on two-sides are shown in (4) and (5).

$$I_{ds\_ts} = -I_{tr} + I_{mag\_r} \tag{4}$$

$$I_{ds\_tr} = -I_{tr} - I_{mag\_r} \tag{5}$$

The I_{tr} should meet the following condition so that the current will discharge the junction capacitors of devices on both sides.

$$|I_{tr}| < 0.5 |I_{mag}| \tag{6}$$

According to (4) and (5), $|I_{ds\_ts}|<|I_{ds\_tr}|$ during the dead-time. Therefore, the receiving-side will finish the voltage transition at T3, faster than the sending-side. As shown in Fig. 9, when the receiving-side finishes the transition, it will apply a reversed voltage across the transformer terminals on the receiving-side. This will drive the I_{tr} to decrease and then reverse the direction, which helps accelerate and finish the voltage transition on the sending-side at T4.

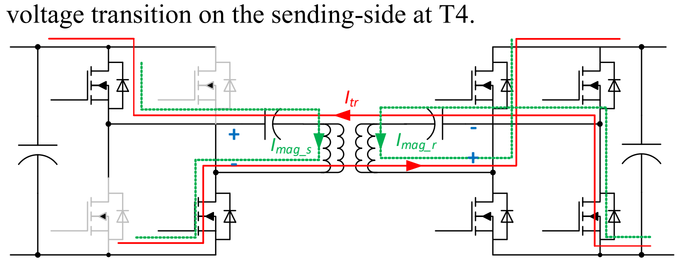

Fig. 9: Current path for bi-directional resonant converter when the receiving-side finishes the voltage transition during dead-time.

When both sides finish the voltage transition, the involved bottom devices are turned on, achieving ZVS.

The above analysis shows that the continuous resonant current contributes to the voltage transition in addition to magnetizing current. With that said, the zero-voltage soft-switching might not be guaranteed at the heavy load condition (larger I_{tr}). Fig. 10 shows a waveform when twice the current shown in Fig. 6 is delivered. As discussed in (4), the sending-side current will be smaller at T2 moment thereby taking longer time, even longer than dead-time, to finish the voltage transition. This leads to non ZVS switching on the sending-side bottom device. At the heavy load condition, I_{tr} can be so large that I_{ds_ts} <0. The voltage transition on the sending-side will not start during dead-time until the receiving-side finishes the transition. This will take a much longer time for sending-side to finish the voltage transition.

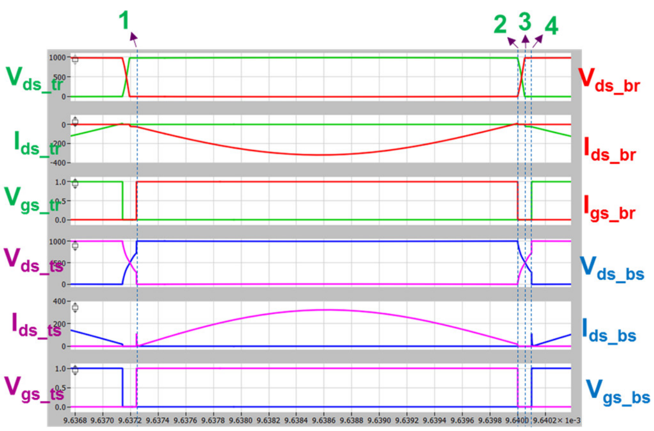

Fig. 10: Non ZVS at sending-side under heavy load condition.

The soft-switching transition and design rules for the bi-directional resonant dc-dc converter are different from the typical LLC circuit and are summarized as follows.

1. Both sides will supply the transformer magnetizing current and the magnetizing current should be designed enough to discharge devices from both sides.

2. The resonant current will contribute to the devices voltage transition during dead-time. When the switching frequency is equal or lower than the resonant frequency, the receiving-side will finish devices voltage transition first. Sending-side devices have a higher chance to lose soft-switching.

3. The worst case to design magnetizing current and dead-time happens at the full-load condition. Therefore, the tuning should be conducted at full-load condition.

It should be noted that if the switching-frequency is intentionally tuned higher than the resonant frequency, the sending-side will finish the switching transition sooner than the receiving-side. Due to the medium voltage insulation across the transformer, fiber optics are the typical media to send gate-signals. Therefore, as shown in Fig. 11, the delay due to fiber interface should be considered and compensated to ensure alignment of gating-signals on two-sides.

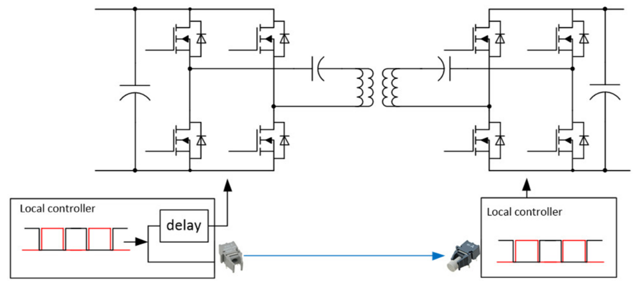

Fig. 11: Practical implementation with fiber optics.

B. Transformer Winding Current Analysis

The high-frequency transformer delivers single-phase power. A simple model as shown in Fig. 12 can be used to study the operation. The hard-switching H-bridge behaves like a current source I_{line} to inject or sink pulse current to the dc-dc stage. The dc-link capacitor provides filtering of both switching current I_{line} from hard-switched line-bridge and switching current I_{inner} from soft-switched inner-bridge. As f_{sw_l} << f_{sw_i}, the floating dc-link voltage ripple $v_{dc\_f\_ripple}$ is dominated by I_{line}. v_{t1} and v_{t2} are the soft-switching H-bridge terminal voltages of which the amplitudes are defined by the dc-link voltages on both sides. The difference between v_{t1} and v_{t2} will drive the transformer winding current. Therefore, the high-frequency transformer winding current harmonic content consists of three major frequency components: double line-frequency (120Hz), double line-bridge switching-frequency ($2*f_{sw\_l}$), and inner-bridge switching-frequency (f_{sw_i}). Therefore, the hard-switched switching frequency f_{sw_l} will impact the I_{tr} waveform, and ultimately the RMS value. Fig. 13 shows one-line period of transformer current simulation result with f_{sw_i} = 180 kHz, C_{dc_f} = 50uF, v_{dc_f} = 1 kV. Several waveforms under different line-bridge switching-frequency f_{sw_l} = 2 kHz, 6 kHz, and 12 kHz are compared. Table II shows the transformer winding current RMS and winding loss values, indicating that there are more than 20% higher RMS current and 45% higher winding losses under lower line-bridge switching-frequency.

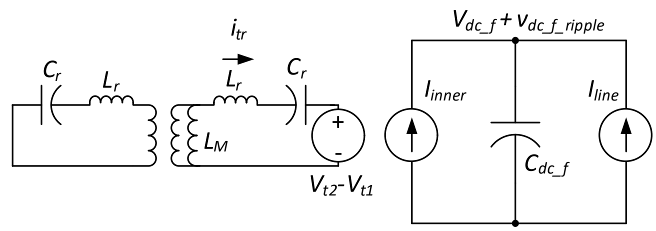

Fig. 12: Simplified model of PEBB.

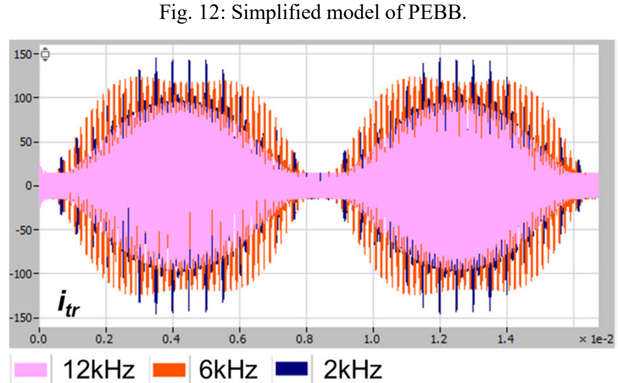

Fig. 13: High-frequency transformer current.

Table II Switching frequency in modular SST PEBB

f_{sw_l}	I_{tr} RMS value (p.u.)	Winding loss (p.u.)
12 kHz	1	1
6 kHz	1.154	1.33
2 kHz	1.204	1.45

Therefore, in order to reduce the winding RMS current, line-bridge f_{sw_l} should be higher or the floating dc-link should have a larger dc-link capacitor.

C. Controller Architecture and Protection

Due to the complexity of SST-based converter system, each module has to contain a local FPGAs and local sensing on gate-drivers to generate gate-signals. The daisy-chain fiber connection is used for central controller to control the system with any number of the SST modules [23]. A "syn" signal is looped for the central controller to synchronize all modules and toggle the state-machine. The fault-signal is looped as well so that any faulty module can trip the entire system.

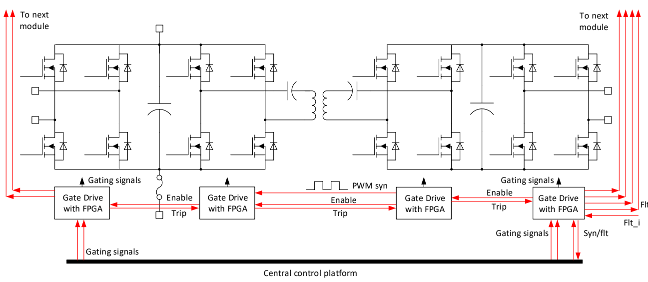

Fig. 14: Control architecture with daisy-chain based control signal distribution.

Each local controller has a dc-link over/under voltage protection, auxiliary power protection, de-sat protection. All modules are paralleled at the low-voltage side to share a single dc-link bus. Each module contains a fast-acting dc fuse. If any of the modules have an internal short-circuit fault. Dc-link capacitors from all modules will dump the energy though the faulty-module fuse, which in turn opens the fuse and isolated the fault.

III. Hardware Design Consideration

Hardware design and its packaging solution is critical to the MV modular SST in order to optimize insulation clearance, ease of cooling, and power/weight density. The power electronics power stage design in SST should consider multiple inter-connected factors, as shown in Fig. 15, driven in large by the transformer frequency and power rating. As shown in Table III, 50 kVA rating per module is selected to build a 6 kV MV class 1 MVA converter system for applications like doubly-fed induction generator (DFIG) wind converter system.

Table III Three-phase 6kV to 1kV ac-ac converter system rating

Modular SST rating	50 kVA
Single SST output	690 V
Total Number of modules with N+1 redundancy per phase	6
Total power rating	~1MVA
Medium-voltage three-phase ac voltage	6 kV

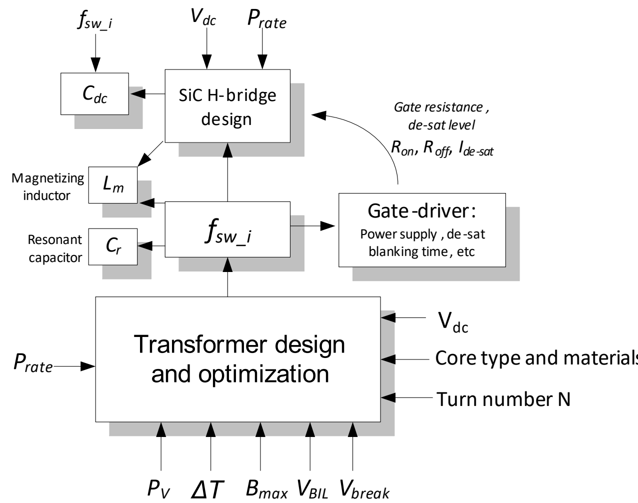

Fig. 15. Converter hardware design trade-off

For MV insulated transformer, its power rating will be limited by the primary-side winding ampere rating. Higher terminal voltage helps increase the power rating and thereby power density. Therefore, the dc-link voltage must be higher than 1 kV and 1.7 kV SiC MOSFETs, as shown in Table IV are selected in the design.

Table IV: Data of SiC MOSFETs used in design

Vendor	Wolfspeed
Part-number	XPM3-1700-0020B
Package	TO247-4L
R_{dson}	R_{dson} = 20mΩ@25ºC R_{dson} =42mΩ@175ºC
Selected Gate-resistance	R_{on} = 10 Ω, R_{off} = 10 Ω
Gate-source voltage	V_{on} = 15V, V_{off} = -5V

The core material (3C98) [24] core-loss were characterized and the operational frequency f_{sw_i} is selected around 200 kHz at close to 100ºC core temperature, which presents the best core-loss density. The switching-frequency and power rating will determine the number of paralleled devices given its switching loss characterization, cooling condition as well as gate-driver design [25].

The discrete devices are selected due to its most available packaging options and the switching speed can be pushed above 30 V/ns with minimized switching stresses [25]. The packaging options were evaluated between TO-268 surface-mount type and TO-247 lead-type during the design phase from cost, assembly, and cooling perspectives. Up to four devices can be paralleled on the designed PCB circuit, and the layout is meticulously designed to minimize the switching loop without adding any de-coupling capacitors. As shown in Fig. 16 and 17, both options are built and evaluated in the electrical test.

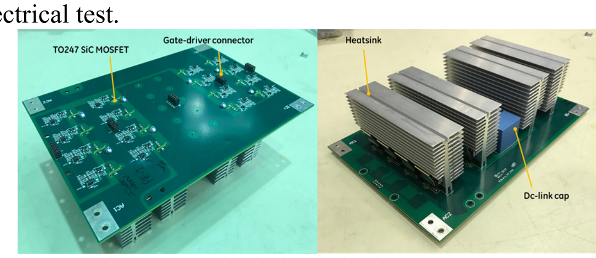

Fig. 16: PCB-based air-cooled high-speed H-bridge using TO-247 devices.

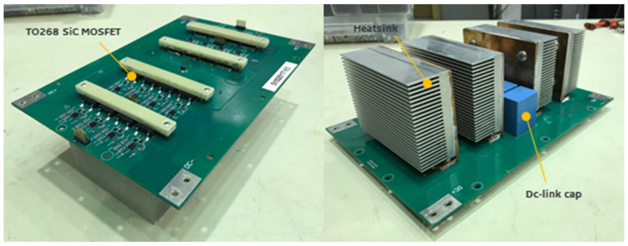

Fig. 17: PCB-based air-cooled high-speed H-bridge using TO-268 devices.

Both solutions present their benefit and penalty. TO-268 based power board can be potentially manufactured via automated process by using thermal reflow solution. On the other hand, the heat-loss has to be transferred vertically through PCB board by multiple thermal vias, leading to worse thermal performance. As shown in Fig. 18, there is about 20°C device temperate difference between TO-247 and TO-268 under 11 W/device, 50°C ambient temperature, and 4 cubic feet per minute (CFM) air-flow conditions. More thermal discussion will be addressed in a separate paper.

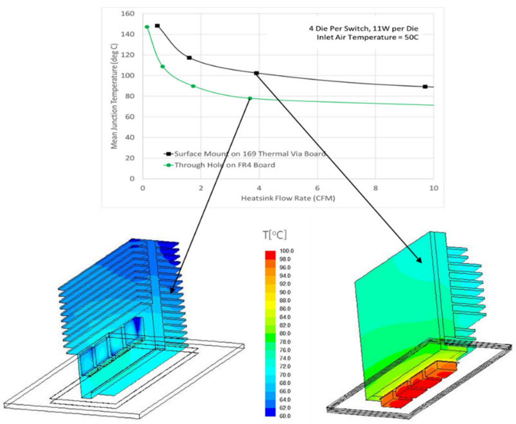

Fig. 18: Simulation of device cooling for through hole and SMD devices.

The module packaging is designed based on an open-frame rail structure, which can be lifted by two people. The MV-side power electronics circuits are connected to the rails by MV glastic insulators. The back-back power electronics circuits are inter-connected in a sandwich structure where the heatsinks face toward outside in a way that centralized top-blower can extract the heat vertically. No local fans are needed. The air ducts are placed within the converter cabinet to guide the most air through the heatsink.

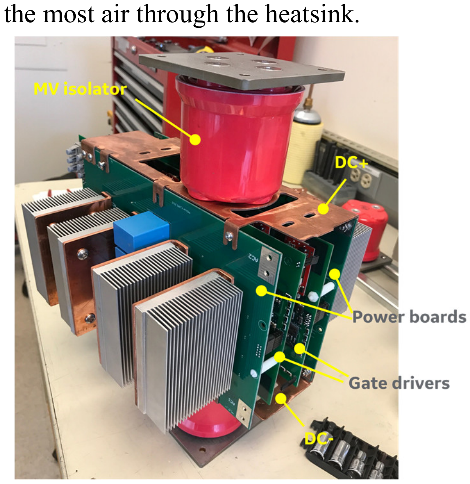

Fig. 19: Sandwich packaging structure.

The high frequency air-cooled transformer design involves the trade-off among thermals, insulation system and structure, core/winding loss, manufacturability, and size. As shown in Fig. 20, the transformer is designed with 6 set of 3C98 ferrite cores, primary and secondary are each made using 2 parallel windings with 4 turns on each winding. Plenary structure is chosen to minimize the leakage inductance and high-frequency ac losses.

The MV insulation system used in the proposed design is based on polymer composite materials involving multiple polymer and inorganic components. With a proper selection of materials combination and geometric arrangement, a void-free insulation can be achieved with effective thermal conductivity of greater than 0.8 W-m/K, and breakdown strength of about 60 kV/mm under impulse voltages. The surface of the primary insulation is covered by a semi-conductive shield connected to ground. Semiconductor nonlinear stress grading material (SGM) is applied around the primary winding terminals to carefully manage the electric-stress around the terminal edges. Sufficient turn insulation is also included for both windings. Fig. 20 and 21 show the MV-insulated winding prototype and bushing and barriers for striking distance. The size comparisons between single-phase 60 Hz and 200 Hz transformers with the same power and BIL ratings are shown in Fig. 21 (b). More details on transformer design can be referred to [26].

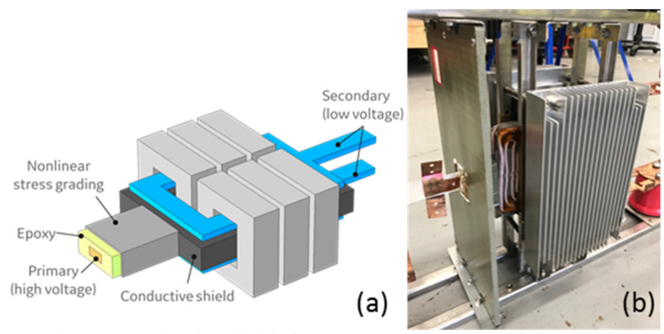

Fig. 20: MV insulated high-frequency transformer (a) design layout, (b) bushing and barrier.

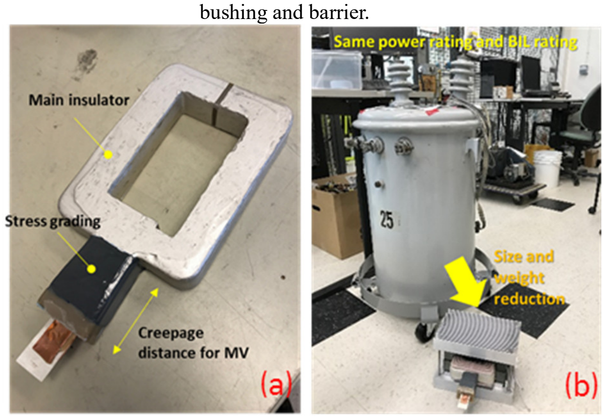

Fig. 21: (a) MV insulated winding prototype, (b) comparison between 60 Hz transformer and 200 kHz transformer.

IV. Experiments Evaluation

Figure 22 shows the final 50 KVA MV-insulated (6kV) ac-ac modular SST assembly. Fig. 23 shows the test setup to test and characterize the module and Fig. 24 shows the electric circuit diagram of the module test setup, where ac terminals of the two-line side converters are connected through a 2 mH inductor and the circulating current within the module is regulated using the phase shift angle between the ac voltages of the two line-side bridges. The external dc power supply only delivers the system losses. The test conditions are listed in Table V and Fig. 25 shows the 45 kW power pump-back test waveforms on the ac line-side and the resonant tank voltage and current, with line-side fundamental ac waveforms set to 60 Hz. In Fig. 26, the resonant voltages on primary and secondary bridges are shown with the resonant current. The turn on transition occurs at negative current, therefore ZVS is achieved and because the operation is only very slightly below the resonant frequency, turn off transition occurs when the SiC MOSFET is carrying only the magnetizing current plus very small resonant current. Therefore, the turn off loss is very low. Fig. 27 shows the ac-ac converter efficiency under two hard-switching frequency conditions: 2 kHz and 4 kHz. The efficiency exceeds 98% at the 2 kHz condition. The loss breakdown based on combined test results and thermal models are shown in Fig. 28. The line bridges exhibit turn on, turn off and conduction losses, increasing the line bridge switching frequency from 2 kHz to 4 kHz leads to a 0.2% drop in efficiency. Whereas, the inner high frequency bridges operating at 180 kHz, exhibit mainly conduction losses due to the soft switching achieved by the resonant circuit.

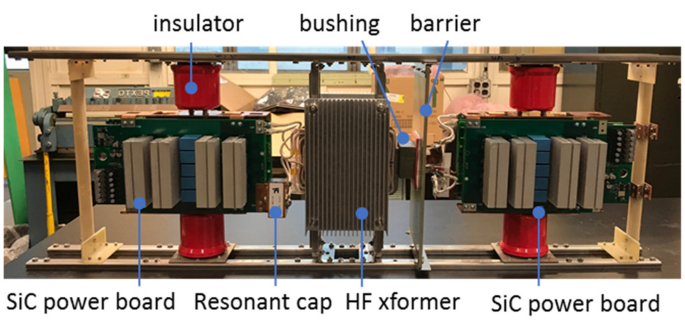

Fig. 22: Final MV SiC SST module assembly.

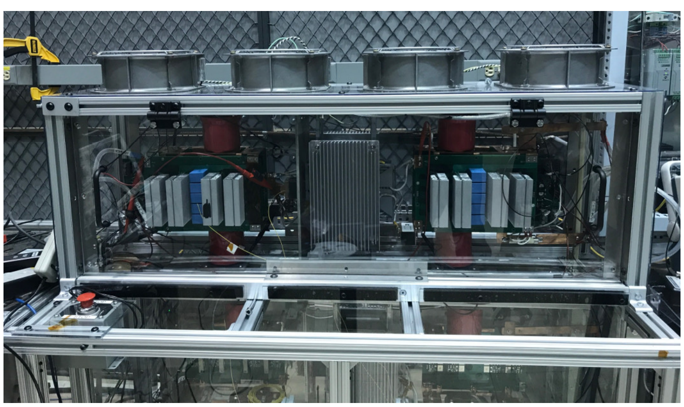
Fig. 23: Single module pump-back test setup.

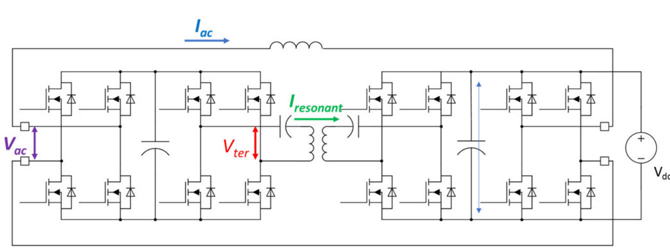

Fig. 24: Single module pump-back test diagram.

Table V: Test condition

Dc-link voltage	1.1kV
Inner bridge switching frequency	180 kHz
Outer bridge switching frequency	2kHz, 4kHz
Device in parallel in inner bridge	2
Device in parallel in outer bridge	4
Ac output voltage	690 Vrms
Ambient temperature	21 ºC
Dc-link capacitance	50 µF

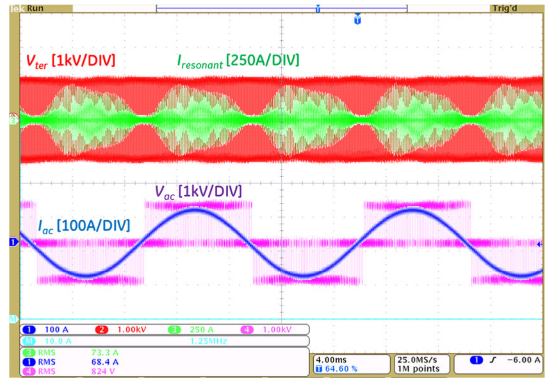

Fig. 25: 45 kW ac-ac SST module pump-back test waveform.

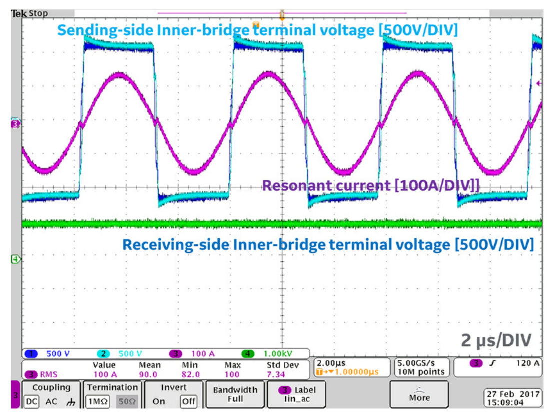

Fig. 26: High-frequency inner-bridge resonant current and terminal voltage.

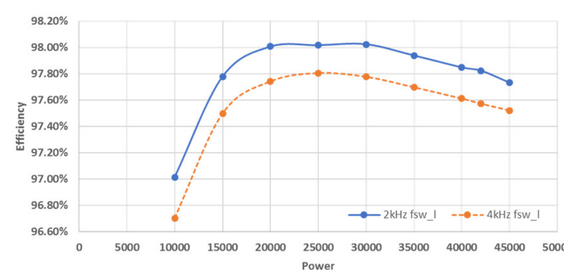

Fig. 27: Efficiency curve with different hard-switching frequency.

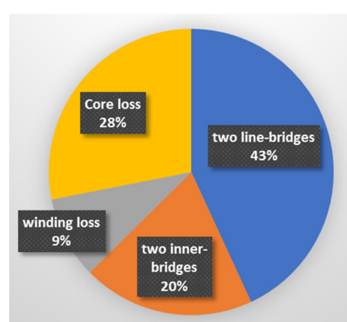

Fig. 28: Preliminary loss breakdown characterization result at 42kW with 4kHz hard-switching frequency.

Figure 29 and 30 shows the high-frequency transformer current waveform under three different outer-bridge switching frequencies: 12kHz, 2kHz, respectively, showing the strong coupling between winding current and the outer-bridge switching-frequency. Higher outer-bridge frequency generates smaller transformer current harmonic contents, thereby lower winding losses and audible noises.

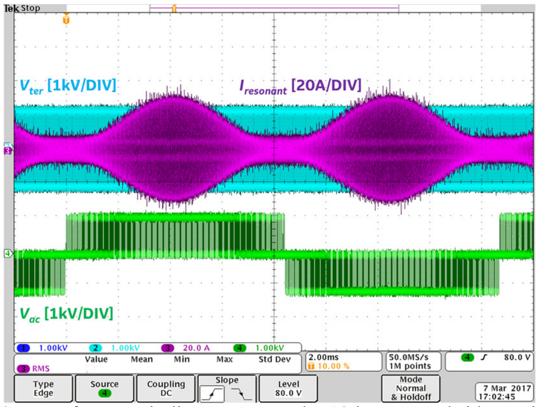

Fig. 29: Transformer winding current under 12 kHz outer-bridge switching frequency.

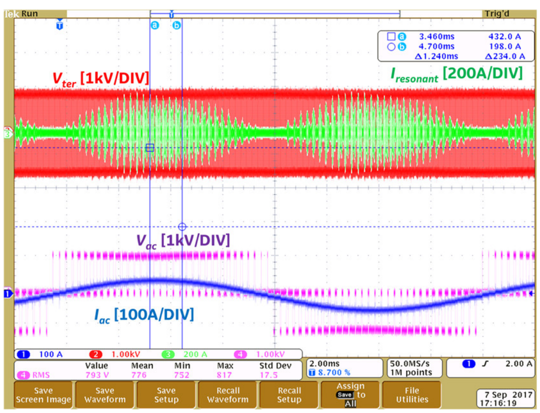

Fig. 30: Transformer winding current under 2 kHz outer-bridge switching frequency.

Several identical SiC SST modules are fabricated for MV voltage converter system. Fig. 31 shows a test setup built by cascading two modules in series to run a two-by-two pump-back test, with the circuit diagram for the test shown in Fig. 32. Fig. 33 shows that the total ±2.2kV output five-level ac waveform under 90kW pump-back power condition. The output voltage can be scaled up as shown in Fig. 34 where 4 modules are stacked in series with a resultant 9-level ac line voltage of 4.4 kV peak voltage. In this case, with 4 series modules at line bridge switching frequency of 2 kHz, the effective output switching frequency is 16 kHz.

Fig. 31. Two-by-two pump-back test in cabinet environment

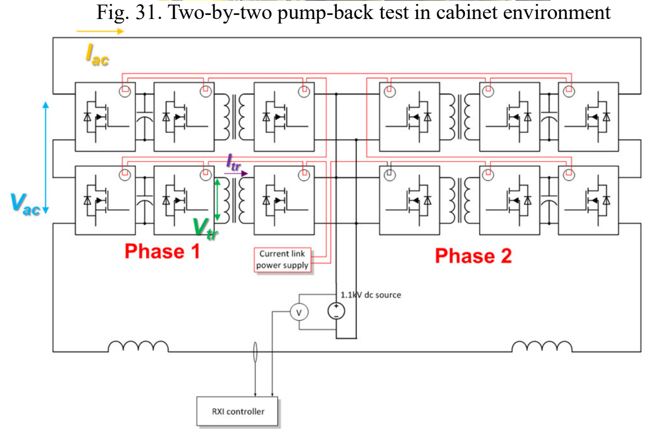

Fig. 32: 2×2 SST-based converter single-phase pump-back test diagram.

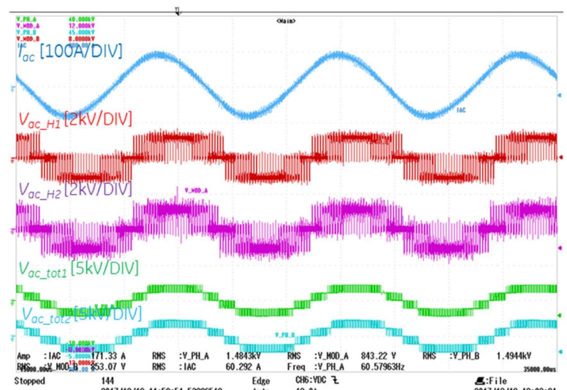

Fig. 33: Two-by-two pump-back test result.

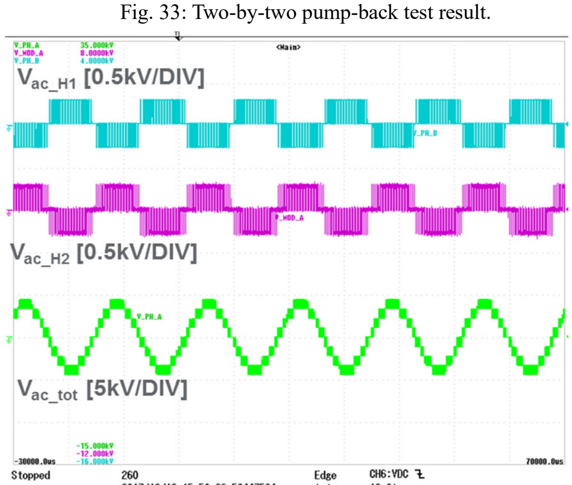

Fig. 34: Output waveforms with four series modules.

V. Conclusions

In this paper, a modular, high power, high frequency SiC solid-state transformer is presented for MV grid application. Converter implementation is based on discrete SiC MOSFETs that are soft switched in the Solid-State Transformer stage and hard switched in the rectifier/inverter stages. Operating at 180 kHz enables the use of ferrite cores and fewer number of transformer turns. However, to maintain high conversion efficiency and low component stress, a resonant SST is used and the SiC devices achieve soft switching at turn on and close to soft turn off as they only interrupt the transformer magnetizing current. The bi-directional operational mode, control, and transformer winding current are analyzed. The hardware design and packaging solution are presented. An SST efficiency of ~98% is achieved with an overall module efficiency including line bridges exceeding 98%. The proposed methods have been verified using 50 kVA SiC SST modules.

Acknowledgement

This work was supported in part by the U.S. Department of Energy under Grant DE-EE0007252. This report was prepared as an account of work sponsored by an agency of the U.S. Government. Neither the U.S. Government nor any agency thereof, nor any of their employees, makes any warranty, express or implied, or assumes any legal liability or responsibility for the accuracy, completeness, or usefulness of any information, apparatus, product, or process disclosed, or represents that its use would not infringe privately owned rights. References herein to any specific commercial product, process, or service by trade name, trademark, manufacturer or otherwise does not necessarily constitute or imply its endorsement, recommendation, or favoring by the U.S. Government or any agency thereof. The views and opinions of authors expressed herein do not necessarily state or reflect those of the U.S. government or any agency thereof.

References

[1] W. McMurray, "The thyristor electronic transformer: A power converter using a high-frequency link," IEEE Transactions on Industry and General Applications, 1971, vol. IGA-7, no. 4, pp. 451-457.

[2] J. W. Kolar, J. E. Huber, "Solid-state Transformer – Key Design Challenge, Applicability, and Future Concepts," IEEE Applied Power Electronics Conference, 2016.

[3] C. H. Zhao, et al., "Power Electronics Traction Transformer – Medium Voltage Prototype," IEEE Trans. Industrial Electronics, vol., 61, July 2014.

[4] A. J. Watson, P. W. Wheeler, and J. C. Clare, "Field programmable gate array based control of Dual Active Bridge DC/DC Converter for the UNIFLEX-PM project," in Power Electronics and Applications (EPE 2011), Proceedings of the 2011-14th European Conference on, 2011, pp.1-9.

[5] M. Steiner and H. Reinold "Medium frequency topology in railway applications", 12th Eur.Conf. on Power Electron. Appl., 2007.

[6] Ravisekhar Raju, Mark Dame, Robert Steigerwald, "Solid-State Transformer using Silicon Carbide-based Modular Building Blocks," IEEE International Conference on Power Electronics and Drive Systems (PEDS), 2017.

[7] A.Q. Huang, "Medium-Voltage Solid-State Transformer: Technology for a Smarter and Resilient Grid," IEEE Industrial Electronics Magazine, Sept. 2016, pp. 29-42.

[8] Engel, M. Victor, G. Bachmann, "15kV/16.7Hz energy supply system with medium frequency transformer and 6.5 KV IGBTs in resonant operation," European Conference on Power Electronics and Applications (EPE), 2001.

[9] L. Heinemann, "An actively cooled high power, high frequency transformer with high insulation capability," IEEE Applied Power Electronics Conference (APEC), 2002.

[10] Zhao, M. Weiss, A. Mester, S. Lewdeni-Schmid, D. Dujic, J. Steinke, T. Chaudhuri, 'Power electronic transformer (PET) converter: Design of a 1.2 MVA demonstrator for traction application', International Symposium on Power Electronics, Electrical Drives, Automation and Motion (SPEEDAM), 2012.

[11] M. Agamy, D. Dong, L.J. Garces, Y. Zhang, M. Dame, A.S. Atalla, Y. Pan, "A high power medium voltage resonant dual active bridge for DC distribution networks," *IEEE Energy Conversion Congress and Exposition (ECCE)*, 2016.

[12] Amorphous and Nanocrystalline Materials: Finemet™, Hitachi; http://www.hitachimetals.com.

[13] S. Zhao, Q. Li, F.C. Lee, "High frequency transformer design for modular power conversion from medium voltage AC to 400V DC," IEEE Applied Power Electronics Conference (APEC), 2017.

[14] IEEE Std. C57.12.01-2015 "IEEE Standard for General Requirement for Dry-Type Distribution and Power Transformers,"

[15] J. H. Jung, H. S. Kim, M. H. Ryu, J. W. Baek, "Design Methodology of Bidirectional CLLC Resonant Converter for High-Frequency Isolation of DC Distribution Systems," IEEE Trans. Power Electronics, vol. 28, pp. 1741-1755, April 2013.

[16] W. Chen, P. Rong, Z. Lu, "Snubberless Bidirectional DC–DC Converter With New CLLC Resonant Tank Featuring Minimized Switching Loss," IEEE Trans. Industrial Electronics, vol. 57, pp. 3075-3086, Sept. 2010.

[17] B. Li, Q. Li, F. C. Lee, "A WBG based three phase 12.5 kW 500 kHz CLLC resonant converter with integrated PCB winding transformer," IEEE Applied Power Electronics Conference and Exposition (APEC), pp. 469-475, 2018.

[18] J. Huang, et al., "Robust Circuit Parameters Design for the CLLC-Type DC Transformer in the Hybrid AC/DC Microgrid," IEEE Transactions on Industrial Electronics, 2018.

[19] R. W. DeDonker, D. M. Divan, and M. H. Kheraluwala, "A three-phase soft- switched high power density dc-dc converter for high power applications," IEEE Trans. Ind. Applications., vol. 27, pp. 63–73, Jan./Feb. 1991.

[20] B. Zhao, Q. Song, W. Liu, Y. Sun, "Overview of Dual-Active-Bridge Isolated Bidirectional Dc-Dc Converter for High-frequency-Link Power-Conversion System," IEEE Trans. Power Electronics, vol. 29, pp. 4091-4106, Aug. 2014.

[21] F. Z. Peng, H. Li, G. J. Su, J. S. Lawler, "A New ZVS Bidirectional DC-DC Converter for Fuel Cell and Battery Application," IEEE Trans. Power Electronics, vol. 19, pp. 54-65, Jan. 2004.

[22] W. Feng, P. Mattavelli, F. C. Lee, D. Fu, "LLC converters with automatic resonant frequency tracking based on synchronous rectifier (SR) gate driving signals," IEEE Applied Power Electronics Conference and Exposition (APEC), 2011.

[23] D. Dong, R. Raju, G. Ganireddy, M. Agamy, "Rotational Control Method with Transformer Loss Savings in Solid-state Transformer based Converter System", IEEE Energy Conversion Congress and Exposition (ECCE), 2018.

[24] Ferrite Materials for Power Conversion, Ferroxcube, https://www.ferroxcube.com/upload/media/product/file/MDS/3c98.pdf.

[25] D. Dong, M. Agamy, G. Mandrusiak, Q. Chen, "Design of High-Speed H-bridge Converter Using Discrete SiC MOSFETs for Solid-State Transformer Applications," IEEE Energy Conversion Congress and Exposition (ECCE), pp. 1379-1386, 2017.

[26] Q. Chen, R. Raju, D. Dong, M. Agamy, "High Frequency Transformer Insulation in Medium Voltage SiC enabled Air-cooled Solid-State Transformer," IEEE Energy Conversion Congress and Exposition (ECCE), 2018.